

The QCD corrections to scalar top pair production in photon-photon collisions *

CHANG Chao-Hsi^{a,b}, HAN Liang^c, MA Wen-Gan^{a,b,c} and YU Zeng-Hui^{c,d}

^aCCAST (World Laboratory), P.O.Box 8730, Beijing 100080, China.[†]

^bInstitute of Theoretical Physics, Academia Sinica,
P.O.Box 2735, Beijing 100080, China.

^cDepartment of Modern Physics, University of Science and Technology
of China (USTC), Hefei, Anhui 230027, China.

^dInstitut für Theoretische Physik, Universität Wien, A-1090 Vienna, Austria

Abstract

The complete QCD corrections to the scalar top quark pair production via $\gamma\gamma$ fusion in parent e^+e^- collider are calculated in the Supersymmetric Model. The various origins of corrections are discussed. We find that the correction due to gluino exchange is smaller than that due to conventional gluonic contribution, and the contribution due to squark quartic interactions is much smaller. Moreover, the dependences of the corrections on the masses and the mixing angle of the supersymmetric particles are also investigated.

PACS number(s): 14.80.Ly, 12.15.Lk, 12.60.Jv

*The project supported by National Natural Science Foundation of China

[†]Not mailing address.

1.Introduction

The Standard Model (SM) [1] [2] has achieved great successes in describing all the available experiment data pertaining to the strong, weak and electromagnetic interaction phenomena up to a few percentage level quantitatively. Only the elementary Higgs boson, required strictly by the Standard Model for spontaneous symmetry breaking, remains to be found. At present the Supersymmetric extended Model (MSSM)[3] is regarded as one of the most attractive model. Apart from containing a large number of experimental consequences, the supersymmetric theory is able to solve various theoretical problems, such as the fact that SUSY maybe provides an elegant way to construct the huge hierarchy between the electroweak symmetry-breaking scale and the grand unification scales.

One of the most important consequence of the SUSY model is to predict the existence of scalar partners to all existing fermions in the SM. In the model two coloured scalar quarks (squarks) \tilde{q}_L and \tilde{q}_R are required as partners of the standard Dirac quarks. To probe the existence of these squarks, to look for pair production $\tilde{q}\tilde{q}^*$ would be a very promising. The pair production may have a comparatively large cross section, depending on the masses of the squark. Furthermore, if both pair-produced squarks decay via $\tilde{q} \rightarrow q\tilde{\gamma}$, the signature with hard acoplanar quark jets, may be quite good for detection, allowing identification of individual events which would not occur in the Standard Model.

Since \tilde{q}_L and \tilde{q}_R will turn to their mass eigenstates by mixing with each other if they are produced, and the mixing size is proportional to the mass of the related ordinary quark [4]. As the top quark is very heavy, the scalar partners of top quark (stop quark) are expected

to be strongly mixed. Therefore, one of the two mass eigenstates of stop quarks \tilde{t}_1 and \tilde{t}_2 , which are mixtures of the left and right weak eigenstates of the stops \tilde{q}_L and \tilde{q}_R , may be comparative light (the lightest one of the all squarks) i.e. we may suppose the one of the stop mass eigenstates \tilde{t}_1 is much lighter than the other one \tilde{t}_2 . As a result, \tilde{t}_1 is very possible to be discovered in a relatively low energy range.

The Next-generation Linear Collider (NLC) is designed to look for the evidences of Higgs and other new particles beyond the Standard Model. To detect the existence of the heavy squarks, e^+e^- collision has advantage over pp or $p\bar{p}$ collision with its cleaner background. Squark pair production produced by e^+e^- annihilation has been studied thoroughly, both at tree level [5] and at next-to-leading [6]. The overall consideration of producing a scalar top pair via $\gamma\gamma$ collision is still absent and its production rate may be greater than that by the e^+e^- annihilation as the later has an ‘s-channel suppression’ due to the virtual photon propagator when the scalar top quark is so heavy. Moreover, in the process of squark pair production via photon fusion, the final particles should not be two different squark mass eigenstates, because it is merely electromagnetic interaction phenomenon and no weak interaction is involved at the tree-level, other than in the production of $e^+e^- \rightarrow \tilde{q}_i\bar{\tilde{q}}_j$ ($i, j = 1, 2$) there must be some contribution from Z boson exchange. Therefore, $\gamma\gamma$ collision provides another interesting mode of producing squark pair which is worthwhile to investigate. Furthermore, with the advent of new collider technique, the NLC is not only able to work as e^+e^- collider, but also to turn the high energy electron-positron beams into the Compton backscattering energetic photon beams with high efficiency [7]. The luminosity

and energy of the photon collider can be expected to be comparable to those of the primary e^+e^- collision. Therefore, with the solid support of new experimental techniques, there is possibility to yield a scalar top quark pair production directly via the high energy photon collision.

From the above argument we can see that the process of squark pair production via photon-photon collisions would be interesting and will be accessible experimentally. We know that the study for this process only at the tree-level is far from enough in high precision. In this work, we will investigate the 1-loop QCD corrections up to the order $O(\alpha_s)$, including the conventional ones (virtual and real gluon exchange) and those of supersymmetric partners. The paper is organized as follows: In Sec.II the analytical formula of tree level is presented. The different origins of supersymmetry QCD corrections are discussed in Sec.III. In Sec.IV, the numerical results are depicted, and some discussions are given. Finally, the conclusions are made. In the Appendix, the form factors appearing in the cross section of Sec.III are listed.

II. Tree level result

In this work, we denote the reaction of stop quark pair production via photon-photon collision as

$$\gamma(p_3, \mu)\gamma(p_4, \nu) \longrightarrow \tilde{t}_i(p_1)\tilde{\bar{t}}_i(p_2) \quad (2.1)$$

where p_1 and p_2 represent the momenta of the outgoing scalar top-quark and its anti-particle,

p_3 and p_4 describe the momenta of the two incoming photons.

The Feynman diagrams for the process at the tree level are shown in Fig.1-a, and the relevant Feynman rules can be found in [4]. The corresponding Lorentz invariant matrix element of the lowest order for the reaction $\gamma\gamma \rightarrow \tilde{t}_i\bar{\tilde{t}}_i$ is written as

$$M_0 = M_0^{\hat{t}} + M_0^{\hat{u}} + M_0^{\hat{q}} \quad (2.2)$$

where $M_0^{\hat{t}}$, $M_0^{\hat{u}}$ and $M_0^{\hat{q}}$ represent the amplitudes of the t-channel, u-channel and quartic coupling diagrams respectively. The explicit expressions can be given as

$$\begin{aligned} M_0^{\hat{t}} &= \frac{4ie^2Q_{\tilde{t}}^2}{\hat{t} - m_{\tilde{t}_i}^2} \epsilon_\mu(p_3)\epsilon_\nu(p_4) p_1^\mu p_2^\nu \\ M_0^{\hat{u}} &= \frac{4ie^2Q_{\tilde{t}}^2}{\hat{u} - m_{\tilde{t}_i}^2} \epsilon_\mu(p_3)\epsilon_\nu(p_4) p_1^\nu p_2^\mu \\ M_0^{\hat{q}} &= 2ie^2Q_{\tilde{t}}^2 g^{\mu\nu} \epsilon_\mu(p_3)\epsilon_\nu(p_4) \end{aligned} \quad (2.3)$$

The Mandelstam variables \hat{t} and \hat{u} are defined as $\hat{t} = (p_1 - p_3)^2$, $\hat{u} = (p_1 - p_4)^2$. $m_{\tilde{t}_i}$ ($i = 1, 2$) and $Q_{\tilde{t}_i}$ denote the masses and the charge of scalar top quarks respectively.

The cross section at tree level can be depicted as

$$\hat{\sigma}_B[\gamma\gamma \rightarrow \tilde{t}_i\bar{\tilde{t}}_i] = \frac{4\pi\alpha^2}{\hat{s}} Q_{\tilde{t}_i}^4 N_C \beta \left\{ 1 + \frac{8\mu^4}{1 - \beta^2} + \frac{2\mu^2(1 - 2\mu^2)}{\beta} \log w \right\} \quad (2.4)$$

Here $\mu^2 = m_{\tilde{t}_i}^2/\hat{s}$, the velocity of the scalar top quarks is defined as $\beta = \sqrt{1 - 4m_{\tilde{t}_i}^2/\hat{s}}$. The kinematical variable w is defined as $w = (1 - \beta)/(1 + \beta)$. $N_C = 3$ is the number of colors.

III. SUSY QCD corrections

Since the physical squarks are the mixture of the left- and right-handed weak eigenstates, the stop quark mass eigenstates \tilde{t}_1 and \tilde{t}_2 can be expressed by

$$\tilde{t}_1 = \cos \theta_{\tilde{t}} \tilde{t}_L - \sin \theta_{\tilde{t}} \tilde{t}_R, \quad \tilde{t}_2 = \sin \theta_{\tilde{t}} \tilde{t}_L + \cos \theta_{\tilde{t}} \tilde{t}_R \quad (3.1)$$

where $\theta_{\tilde{t}}$ is the scalar top mixing angle which transforms the scalar top mass eigenstates \tilde{t}_i ($i=1,2$) to the weak eigenstates \tilde{t}_L and \tilde{t}_R . We assume that the scalar top quark mass eigenstates split heavily, namely $m_{\tilde{t}_1} \ll m_{\tilde{t}_2}$. Therefore, in this work we constrain our attention only on the calculation of the $\tilde{t}_1 \tilde{t}_1^*$ pair production.

The Feynman diagrams for the process $\gamma\gamma \rightarrow \tilde{t}_1 \tilde{t}_1^*$ including all the QCD corrections up to the order $O(\alpha_s)$ are depicted in Fig.1. The total cross section with the supersymmetric QCD corrections corresponding to Fig.1 can be denoted as

$$\hat{\sigma} = \hat{\sigma}_B + \hat{\sigma}_{soft} + \delta\hat{\sigma}^{(1-loop)} \quad (3.2)$$

where $\hat{\sigma}_{soft}$ and $\delta\hat{\sigma}^{(1-loop)}$ represent the cross section of soft gluon emission and virtual one-loop QCD corrections respectively.

The one-loop supersymmetric QCD corrections originate from three different sources: the conventional virtual gluonic corrections (see Fig.1-b), those due to the gluino exchange and those due to squark quartic interactions (see Fig.1-d). In order to show the virtual effects from the different sources, we divide the loop corrections into three groups correspondingly. In the calculation, the dimensional regularization and on-mass-shell scheme (OMS) [8] are adopted in doing renormalization, whereas when considering the effects from the soft gluons infrared divergences being regularized by introducing a small non-zero gluon mass is adopted.

3.1 Related self-energy and counterterms.

The unrenormalized self-energy of the scalar top \tilde{t}_1 can be written as the summation of three parts.

$$\Sigma(p^2) = \Sigma_{vir}^{(g)}(p^2) + \Sigma^{(\tilde{g})}(p^2) + \Sigma^{(\tilde{t})}(p^2) \quad (3.3)$$

where $\Sigma_{vir}^{(g)}$, $\Sigma^{(\tilde{g})}$ and $\Sigma^{(\tilde{t})}$ denote the scalar top self-energy parts contributed by the diagrams the virtual gluon(Fig.1-b1), gluino exchange(Fig.1-d1) and the scalar top quartic interactions(Fig.1-d5) respectively. The squark quartic interactions are involved by introducing superpotential of the scalar matter fields [4]. Imposing the OMS renormalization conditions [8], one can get the related renormalization constants to $O(\alpha_s)$ order with the formulas

$$\begin{aligned} \delta M^2 &= \delta M^{2(g)} + \delta M^{2(\tilde{g})} + \delta M^{2(\tilde{t})} = \tilde{R}e\Sigma(m_{\tilde{t}_1}^2), \\ \delta Z &= \delta Z^{(g)} + \delta Z^{(\tilde{g})} + \delta Z^{(\tilde{t})} = -\tilde{R}e \frac{\partial \Sigma(p^2)}{\partial p^2} \Big|_{p^2=m_{\tilde{t}_1}^2}, \end{aligned} \quad (3.4)$$

where $\tilde{R}e$ only takes the real part of the loop integral functions appearing in the self-energies. All the definitions of loop integral functions A , B , C and D used in the paper can be found in Ref.[9].

The three contribution parts of the scalar top \tilde{t}_1 self-energy can be written explicitly as

$$i\Sigma_{vir}^{(g)}(p^2) = -i \frac{g_s^2 C_F}{16\pi^2} \left\{ A_0[m_{\tilde{t}_1}] + 4p^2(B_0 + B_1)[p^2, m_g, m_{\tilde{t}_1}] + m_g^2 B_0[p^2, m_g, m_{\tilde{t}_1}] \right\}, \quad (3.5)$$

$$i\Sigma^{(\tilde{g})}(p^2) = i \frac{g_s^2 C_F}{16\pi^2} d \left\{ A_0[m_t] - (m_{\tilde{g}}^2 + m_t m_{\tilde{g}} \sin 2\theta_{\tilde{t}}) B_0[p^2, m_{\tilde{g}}, m_t] - p^2 B_1[p^2, m_{\tilde{g}}, m_t] \right\}, \quad (3.6)$$

$$i\Sigma^{(\tilde{t})}(p^2) = -i \frac{g_s^2}{12\pi^2} \left\{ A_0[m_{\tilde{t}_1}^2] \cos^2 2\theta_{\tilde{t}} + A_0[m_{\tilde{t}_2}^2] \sin^2 2\theta_{\tilde{t}} \right\}, \quad (3.7)$$

where m_g is denoted as the gluon mass and $d = 4 - \epsilon$ is the space-time dimension.

Note that the self-energy part from stop quartic interaction diagram(Fig.1-d5) expressed in Eq.(3.7), is independent on its momentum squared p^2 . This means the corresponding part of the squark wave function renormalization constant $\delta Z^{(\tilde{t})} = 0$. The other related renormalization constants $\delta Z^{(g)}$, $\delta Z^{(\tilde{g})}$, $\delta M^{2(g)}$, $\delta M^{2(\tilde{g})}$ and $\delta M^{2(\tilde{t})}$ can be obtained by using the expressions of Eq.(3.3 ~ 3.7).

3.2 Renormalized one-loop corrections.

The renormalized one-loop matrix element involves the contributions from all the SUSY QCD one-loop self-energy, vertex, box and quartic interaction diagrams(shown in Fig.1 – (b1 ~ b12) and Fig.1 – (d1 ~ d7)) and their relevant counterterms. It can be written in the form as

$$\begin{aligned} \delta M^{(1-loop)} &= \delta M_{vir}^{(g)} + \delta M^{(\tilde{g})} + \delta M^{(\tilde{t})} \\ &= ie^2 Q_{\tilde{t}}^2 \epsilon_{\mu}(p_3) \epsilon_{\nu}(p_4) [f_1 g^{\mu\nu} + f_2 p_1^{\mu} p_1^{\nu} + f_3 p_1^{\mu} p_2^{\nu} + f_4 p_2^{\mu} p_1^{\nu} + f_5 p_2^{\mu} p_2^{\nu}], \end{aligned} \quad (3.8)$$

with

$$f_i = f_{vir,i}^{(g)} + f_i^{(\tilde{g})} + f_i^{(\tilde{t})}, \quad (3.9)$$

where $\delta M_{vir}^{(g)}$ represents the gluon correction part of the one-loop renormalized amplitude, and $\delta M^{(\tilde{g})}$, $\delta M^{(\tilde{t})}$ represent the gluino exchange and the squark quartic interactions contribution respectively. All the renormalized self-energy, vertex, box and quartic interaction loop corrections due to the different sources, are summarized in Lorentz invariant factors $f_{vir,i}^{(g)}$, $f_i^{(\tilde{g})}$ and $f_i^{(\tilde{t})}$ ($i = 1, 5$), respectively. By using this formulation we are to show a clear

distinction among those three different origins of supersymmetry QCD corrections. The explicit expressions of form factors can be found in Appendix.

Now we can achieve the one-loop SUSY QCD corrections of the cross section for this subprocess in unpolarized photon collisions.

$$\begin{aligned}
\delta\hat{\sigma}^{(1-loop)}(\hat{s}) &= \frac{N_C}{16\pi\hat{s}^2} \int_{\hat{t}^-}^{\hat{t}^+} d\hat{t} \, 2Re \sum_{spins}^- \left(M_0^\dagger \cdot \delta M^{(1-loop)} \right) \\
&= \delta\hat{\sigma}_{vir}^{(g)} + \delta\hat{\sigma}^{(\tilde{g})} + \delta\hat{\sigma}^{(\tilde{t})} \\
&= \delta\hat{\sigma}_{vir}^{(g)} + \delta\hat{\sigma}^{(\tilde{g}+\tilde{t})},
\end{aligned} \tag{3.10}$$

where $\hat{t}^\pm = (m_{\tilde{t}_1}^2 - \frac{1}{2}\hat{s}) \pm \frac{1}{2}\hat{s}\beta$. The bar over the sum recalls averaging over initial spins. The correction $\delta\hat{\sigma}^{(\tilde{g}+\tilde{t})} = \delta\hat{\sigma}^{(\tilde{g})} + \delta\hat{\sigma}^{(\tilde{t})}$ will be used to denote the corrections arising from the pure supersymmetric particle contribution.

3.3 Real gluon emission

The real gluon emission diagrams for the process $\gamma\gamma \rightarrow \tilde{t}_1\bar{\tilde{t}}_1g$ are drawn in *Fig.1-c1 ~ c7*.

The cross section of real gluon emission is deduced as

$$\sigma_{real} = \frac{N_c}{4} \frac{1}{2\hat{s}(2\pi)^5} \int \frac{d^3\vec{p}_1}{2E_1} \frac{d^3\vec{p}_2}{2E_2} \frac{d^3\vec{k}}{2\omega} \delta^4(p_3 + p_4 - p_1 - p_2 - k) \sum_{spins}^- |M_{real}|^2 \tag{3.11a}$$

with

$$\begin{aligned}
\sum_{spins}^- |M_{real}|^2 &= C_F g_s^2 \sum_{spins}^- \left(f_{real}^{\tilde{t}\tilde{t}} \cdot |M_0^{\tilde{t}}|^2 + f_{real}^{\tilde{u}\tilde{u}} \cdot |M_0^{\tilde{u}}|^2 + f_{real}^{\tilde{q}\tilde{q}} \cdot |M_0^{\tilde{q}}|^2 \right. \\
&\quad \left. + 2f_{real}^{\tilde{t}\tilde{u}} \cdot Re(M_0^{\tilde{t}\dagger} M_0^{\tilde{u}}) + 2f_{real}^{\tilde{q}\tilde{t}} \cdot Re(M_0^{\tilde{q}\dagger} M_0^{\tilde{t}}) + 2f_{real}^{\tilde{q}\tilde{u}} \cdot Re(M_0^{\tilde{q}\dagger} M_0^{\tilde{u}}) \right)
\end{aligned}$$

$$(3.11b)$$

where \vec{k} and ω denote the momentum and the energy of the outgoing gluon respectively, and M_0^a ($a = \hat{t}, \hat{u}, \hat{q}$) are the invariant matrix elements of tree level defined above. The factors f_{real}^{ab} ($a, b = \hat{t}, \hat{u}, \hat{q}$) can be found in Appendix.

In the region around $k \sim 0$, the cross section in Eq.(3.11), corresponding to the cross section for a soft gluon being emitted, may be approximately alternated as

$$\left(\frac{d\sigma}{d\Omega}\right)_{soft} = - \left(\frac{d\sigma}{d\Omega}\right)_B \frac{g_s^2 C_F}{(2\pi)^3} [I_{ii} + I_{ij}] \quad (3.12)$$

where

$$I_{ii} = 2\pi \left\{ 2\log\left[\frac{2\Delta E}{m_g}\right] + \frac{\log[w]}{\beta} \right\} \quad (3.13a)$$

$$I_{ij} = 2\pi \frac{1 - 2\mu^2}{\beta} \left\{ 2\log[w]\log\left[\frac{2\Delta E}{m_g}\right] + 2Li_2\left[\frac{2\beta}{1 + \beta}\right] + \frac{1}{2}\log^2[w] \right\} \quad (3.13b)$$

Here a small soft gluon energy cut ΔE is introduced. $Li_2[x]$ is the Spence function. The definition of β is the same as in Eq.(2.4). The expressions Eq.(3.12) and Eq.(3.13a,b) are similar to those as described in Ref.[8] for a soft photon being emitted, that just is a check of Eq.(3.11) for the real gluon emission in a certain sense. However, for the cancellation of the infrared divergences due to gluons, it is sufficient that only the soft gluons, i.e. gluons with energy $\omega \leq \Delta E$, are relevant, where ΔE is small, which may be set to be smaller than all relevant energy scales in concerned problem. Therefore, we adopt the soft gluon approximation method with a cut ΔE in numerical calculations for the soft gluon emission corrections. With this approach the radiation from internal colour lines or quartic vertices does not lead to IR-singularities and can be neglected in this approximation.

The correction to the total cross section from the gluonic QCD contributions should be expressed as below

$$\delta\hat{\sigma}^{(g)} = \delta\hat{\sigma}_{vir}^{(g)} + \hat{\sigma}_{soft} \quad (3.14)$$

IV. Numerical results and discussions

In the numerical evaluation, we take the value of the top-quark mass to be $m_t = 175 \text{ GeV}$, $\alpha = 1/128$ and use the one-loop running coupling constant α_s . We assume $m_{\tilde{t}_1} < m_{\tilde{t}_2}$ for the masses of the stop quark mass eigenstates. The present constraint from experiments[10] is that the lighter scalar top mass eigenstate $m_{\tilde{t}_1}$ should be heavier than 50 GeV.

The corrections to the cross section of the process $\gamma\gamma \rightarrow \tilde{t}_1\bar{\tilde{t}}_1$ as a function of the center-of-mass $\sqrt{\hat{s}}$ are studied with the values of the involved SUSY parameters given below

$$m_{\tilde{t}_1} = 200 \text{ GeV}, \quad m_{\tilde{t}_2} = 550 \text{ GeV}, \quad m_{\tilde{g}} = 250 \text{ GeV}, \quad \cos\theta_{\tilde{t}} = 0.7 \quad (4.1)$$

The results are depicted in Fig.2(a). These results of numerical calculations show (i) Both corrections $\delta\hat{\sigma}^{(g)}$ and $\delta\hat{\sigma}^{(\tilde{g}+\tilde{t})}$ reach their maximal values around the threshold of $\tilde{t}_1\bar{\tilde{t}}_1$ pair production and vary from positive to negative value as increasing $\sqrt{\hat{s}}$. The former varies severely and in general is several times higher than the later. (ii) The relative corrections due to the gluon contribution can even reach +50% when c.m.s energy $\sqrt{\hat{s}}$ is just above the pair threshold, whereas the maximal value of $\delta\hat{\sigma}^{(\tilde{g}+\tilde{t})}/\hat{\sigma}_B$ is only about +10%. Therefore, one may see the fact that the SUSY QCD corrections are dominated by the gluon contributions.

The $\tilde{t}_1\bar{\tilde{t}}_1$ pair production via photon-photon fusion is only a subprocess of the parent e^+e^- linear collider. It is easy to obtain the total cross section for the scalar top quark pair production via photon fusion in the e^+e^- collider, by simply folding the cross section of the subprocess $\hat{\sigma}(\gamma\gamma \rightarrow \tilde{t}_1\bar{\tilde{t}}_1)$ with the photon luminosity.

$$\sigma(s) = \int_{2m_{\tilde{t}_1}/\sqrt{s}}^{x_{max}} dz \frac{dL_{\gamma\gamma}}{dz} \hat{\sigma}(\gamma\gamma \rightarrow \tilde{t}_1\bar{\tilde{t}}_1 \quad \text{at} \quad \hat{s} = z^2s), \quad (4.2)$$

where \sqrt{s} and $\sqrt{\hat{s}}$ are the e^+e^- and $\gamma\gamma$ center-of-mass energies respectively and $dL_{\gamma\gamma}/dz$ is the distribution of photon luminosity, which is expressed as

$$\frac{dL_{\gamma\gamma}}{dz} = 2z \int_{z^2/x_{max}}^{x_{max}} \frac{dx}{x} f_{\gamma/e}(x) f_{\gamma/e}(z^2/x), \quad (4.3)$$

where $f_{\gamma/e}$ is the photon structure function of the electron beam [7, 11]. We take the structure function of the photon produced by the most promising Compton backscattering as [7, 12]

$$f_{\gamma/e}^{Comp} = \begin{cases} \frac{1}{1.8397} \left(1 - x + \frac{1}{1-x} - \frac{4x}{x_i(1-x)} + \frac{4x^2}{x_i^2(1-x)^2} \right), & \text{for } x < 0.83, x_i = 2(1 + \sqrt{2}) \\ 0, & \text{for } x > 0.83. \end{cases} \quad (4.4)$$

The cross sections of the process $e^+e^- \rightarrow \gamma\gamma \rightarrow \tilde{t}_1\bar{\tilde{t}}_1$ versus \sqrt{s} , with the same condition of Eq.(4.1), are depicted in Fig.2(b). There the magnitude of the corrections is also significant for this process and the sign of corrections goes from positive to negative with the increasing of \sqrt{s} . The total cross section involving SUSY QCD corrections shows the weak dependence on the parent c.m.s energy when $\sqrt{s} > 1 \text{ TeV}$. Furthermore, by analysing our numerical data, the whole correction $\delta\sigma/\sigma_B$ can reach +35%.

In Fig.3 the concerned corrections are plotted as functions of the light scalar top mass $m_{\tilde{t}_1}$, with $\sqrt{\hat{s}} = 1000 \text{ GeV}$, $m_{\tilde{t}_2} = 550 \text{ GeV}$, $m_{\tilde{g}} = 250 \text{ GeV}$ and $\cos\theta_{\tilde{t}} = 0.7$. In most regions

of the value $m_{\tilde{t}_1}$, the corrections due to gluonic contributions are much larger than those due to the scalar top quarks and gluino contributions. Around the region of $m_{\tilde{t}_1} \sim 500 \text{ GeV}$ where $\sqrt{\hat{s}}$ just reaches its pair production threshold, the gluonic corrections become positive, whereas they are negative when $\sqrt{\hat{s}}$ is far above the threshold.

In Fig.4 the concerned corrections with various $m_{\tilde{t}_2}$ and $\sqrt{\hat{s}} = 500 \text{ GeV}$, $m_{\tilde{t}_1} = 200 \text{ GeV}$, $m_{\tilde{g}} = 250 \text{ GeV}$, $\cos\theta_{\tilde{t}} = 0.7$ as well, are depicted. Since the heavy stop mass $m_{\tilde{t}_2}$ only appears in the amplitudes of the diagrams involving the squark quartic vertex, the dependence of the corrections on $m_{\tilde{t}_2}$ manifests only in the correction $\delta\hat{\sigma}^{(\tilde{t})}$. The correction $\delta\hat{\sigma}^{(\tilde{t})}/\hat{\sigma}_B$ approaches to zero with the increment of $m_{\tilde{t}_2}$ and the maximal correction is only about -1% . Note that when $m_{\tilde{t}_2} = 550 \text{ GeV}$, the relative correction $\delta\hat{\sigma}^{(\tilde{t})}/\hat{\sigma}_B$ is only -0.2% , whereas in Fig.2(a) the correction $\delta\hat{\sigma}^{(\tilde{t}+\tilde{g})}/\hat{\sigma}_B$ with the same condition is about $+4\%$. That shows $\delta\hat{\sigma}^{(\tilde{t})}$ is always smaller than both $\delta\hat{\sigma}^{(g)}$ and $\delta\hat{\sigma}^{(\tilde{g})}$. Moreover, the curve of the correction due to the squark quartic interactions shown in Fig.4, becomes rather flat in the large $m_{\tilde{t}_2}$ region, which implies the dependence of $\delta\hat{\sigma}^{(\tilde{t})}$ on heavy \tilde{t}_2 is very weak.

The gluino exchange contribution to the cross section is calculated as a function of $m_{\tilde{g}}$. The results can be seen in Fig.5, where the parameters are set as $\sqrt{\hat{s}} = 500 \text{ GeV}$, $m_{\tilde{t}_1} = 200 \text{ GeV}$, $m_{\tilde{t}_2} = 550 \text{ GeV}$ and $\cos\theta_{\tilde{t}} = 0.7$. The curve of the correction $\delta\hat{\sigma}^{(\tilde{g})}/\hat{\sigma}_B$ is nearly parallel to that of the gluon and stop contribution $\delta\hat{\sigma}^{(g+\tilde{t})}/\hat{\sigma}_B$, which reveals that the correction dedicated by the gluino exchange contribution is independent on $m_{\tilde{g}}$, when the mass of gluino becomes heavy.

The dependence of the corrections $\delta\hat{\sigma}^{(\tilde{g}+\tilde{t})}$ on the mixing angle $\cos\theta_{\tilde{t}}$ for $\sqrt{\hat{s}} = 500 \text{ GeV}$, $m_{\tilde{t}_1} = 200 \text{ GeV}$, $m_{\tilde{t}_2} = 550 \text{ GeV}$ and $m_{\tilde{g}} = 250 \text{ GeV}$ is shown in Fig.6. The combined cor-

rection $\delta\hat{\sigma}^{(\tilde{g}+\tilde{t})}/\hat{\sigma}_B$ varies from -3% to $+5\%$. From the figure one can see that the correction will reach its peak values when $\cos\theta_{\tilde{t}} = \pm 0.7$, namely when the SUSY weak eigenstates \tilde{t}_L and \tilde{t}_R are mixed equivalently.

VI. Conclusion

In this work we have calculated the complete $O(\alpha_s)$ order SUSY QCD corrections, including the conventional gluon contribution and the pure SUSY particle contributions as well, to the $\tilde{t}_1\tilde{t}_1$ pair production process via photon-photon fusion in the initial e^+e^- collider.

From the results of numerical evaluation, it is expected that the corrections due to the pure SUSY particle \tilde{t}_i ($i = 1, 2$) and \tilde{g} contributions are smaller than those from the virtual gluon loop diagrams. Among the pure SUSY particle contributions, those due to the squark quartic interactions are much smaller than those due to the gluino exchange with reasonable parameters. The gluonic correction may reach $+50\%$ in the photon fusion subprocess, when $\sqrt{\hat{s}}$ is around the $\tilde{t}_1\tilde{t}_1$ pair production threshold, whereas the corrections there contributed by \tilde{t}_i and \tilde{g} diagrams are only about $+10\%$. The total QCD corrections to the subprocess will be most significant when $\sqrt{\hat{s}}$ is around the pair production threshold. For the cross section of the process $e^+e^- \rightarrow \gamma\gamma \rightarrow \tilde{t}_1\tilde{t}_1$, the SUSY QCD correction at one-loop level can reach 35% . Furthermore, the corrections also show the decoupling with the heavy \tilde{g} and \tilde{t}_2 masses, and the dependence of the QCD corrections on the mixing angle $\theta_{\tilde{t}}$ obviously.

One of the authors, Z.H. Yu, would like to thank the Institute of Theoretical Physics of University Vienna for the warm hospitality extended to him during his stay under the agreement the exchange program(project number: IV.B.12).

Appendix

The form factors $f_i^{(g)}$ due to the gluon contribution can be expressed as

$$\begin{aligned}
f_{vir,1}^{(g)} &= \frac{g_s^2 C_F}{8\pi^2} \left\{ B_0[p_1 + p_2, m_{\bar{t}_1}, m_{\bar{t}_1}] - \right. \\
&\quad \left. ((m_g^2 C_0 + m_{\bar{t}_1}^2 2C_{11}) - 2(p_1 \cdot p_2)(2C_0 + C_{11})) \right. \\
&\quad \left. [p_1, -p_1 - p_2, m_g, m_{\bar{t}_1}, m_{\bar{t}_1}] \right\} \\
&- \frac{g_s^2 C_F}{4\pi^2} \left\{ (B_0[p_1 - p_3, m_g, m_{\bar{t}_1}] - 2C_{24}[p_1, -p_3, m_g, m_{\bar{t}_1}, m_{\bar{t}_1}] + C_{24}[-p_3, -p_4, m_{\bar{t}_1}, m_{\bar{t}_1}, m_{\bar{t}_1}] + \right. \\
&\quad \left. (2(p_1 \cdot p_2)(2D_{27} + D_{311}) + 2(p_1 - p_2) \cdot p_3(D_{312} - D_{313}) - m_g^2 D_{27} - 2m_{\bar{t}_1}^2 D_{311}) \right. \\
&\quad \left. [p_1, -p_3, -p_4, m_g, m_{\bar{t}_1}, m_{\bar{t}_1}, m_{\bar{t}_1}]) + (p_3 \leftrightarrow p_4) \right\} \\
&+ 2\delta Z^{(g)}
\end{aligned} \tag{A1}$$

$$\begin{aligned}
f_{vir,2}^{(g)} &= -\frac{g_s^2 C_F}{4\pi^2} \left\{ (2C_0 + 3C_{11} - C_{12} + C_{21} - C_{23})[p_1, -p_3, m_g, m_{\bar{t}_1}, m_{\bar{t}_1}] \right. \\
&\quad - (C_{12} + C_{23})[-p_3, -p_4, m_{\bar{t}_1}, m_{\bar{t}_1}, m_{\bar{t}_1}] \\
&\quad + (2(D_{312} + D_{313} - D_{27} - 2D_{311}) + \\
&\quad \quad m_g^2(D_{11} - D_{12} + D_{21} - D_{24} - D_{25} + D_{26}) + \\
&\quad \quad 2m_{\bar{t}_1}^2(D_{21} - D_{24} + D_{31} + D_{310} - D_{34} - D_{35}) + \\
&\quad \quad 2(p_1 \cdot p_2)(D_{34} + D_{35} - 2D_{11} + 2D_{12} - 3D_{21} + 3D_{24} + \\
&\quad \quad \quad 2D_{25} - 2D_{26} - D_{31} - D_{310}) + \\
&\quad \quad 2(p_1 - p_2) \cdot p_3(D_{22} - D_{24} + D_{25} - D_{26} - D_{34} + D_{35} + \\
&\quad \quad \quad D_{36} - D_{37} - D_{38} + D_{39})) \\
&\quad \left. [p_1, -p_3, -p_4, m_g, m_{\bar{t}_1}, m_{\bar{t}_1}, m_{\bar{t}_1}] \right\} \\
&+ (p_3 \leftrightarrow p_4)
\end{aligned} \tag{A2}$$

$$\begin{aligned}
f_{vir,3}^{(g)} &= \frac{g_s^2 C_F}{4\pi^2} \frac{1}{(t-m_{\tilde{t}_1}^2)^2} \left\{ A_0[m_{\tilde{t}_1}] + (m_g^2 B_0 + 4t \cdot (B_0 + B_1))[p_1 - p_3, m_g, m_{\tilde{t}_1}] \right\} \\
&- \frac{1}{(t-m_{\tilde{t}_1}^2)^2} \left\{ t \cdot \delta Z^{(g)} - m_{\tilde{t}_1}^2 \delta Z^{(g)} - \delta M^2(g) \right\} \\
&- \frac{g_s^2 C_F}{2\pi^2} \frac{1}{t-m_{\tilde{t}_1}^2} \left\{ (2B_0 + B_1)[p_1, m_g, m_{\tilde{t}_1}] + (2B_0 + B_1)[p_1 - p_3, m_g, m_{\tilde{t}_1}] + \right. \\
&\quad (m_g^2(C_0 + C_{11}) + 4m_{\tilde{t}_1}^2(C_0 + 2C_{11} + C_{21}) - 4C_{24} - \\
&\quad \quad 2(p_1 \cdot p_3)(2C_0 + 3C_{11} + 2C_{12} + C_{21} + 2C_{23})) \\
&\quad \left. [p_1, -p_3, m_g, m_{\tilde{t}_1}, m_{\tilde{t}_1}] \right\} \\
&+ \frac{2}{t-m_{\tilde{t}_1}^2} \delta Z^{(g)} \\
&+ \frac{g_s^2 C_F}{4\pi^2} \left\{ 2(C_{12} + C_{23})[p_1, -p_3, m_g, m_{\tilde{t}_1}, m_{\tilde{t}_1}] + \right. \\
&\quad 2(C_{12} + C_{23})[-p_3, -p_4, m_{\tilde{t}_1}, m_{\tilde{t}_1}, m_{\tilde{t}_1}] - \\
&\quad (2(2D_{27} + D_{311} + D_{312} - D_{313}) + \\
&\quad \quad m_g^2(D_{26} - D_0 - D_{11} - D_{12} + D_{13} - D_{24}) + \\
&\quad \quad 2m_{\tilde{t}_1}^2(D_{25} - D_{11} - D_{21} - D_{24} + D_{310} - D_{34}) + \\
&\quad \quad 2(p_1 \cdot p_2)(2D_0 + 3D_{11} + 2D_{12} - 2D_{13} + D_{21} + 3D_{24} - \\
&\quad \quad \quad D_{25} - 2D_{26} - D_{310} + D_{34}) + \\
&\quad \quad 2(p_1 - p_2) \cdot p_3(D_{12} - D_{13} + D_{22} + D_{23} + D_{24} - D_{25} - \\
&\quad \quad \quad 2D_{26} - D_{310} + D_{36} - D_{38} + D_{39})) \\
&\quad [p_1, -p_3, -p_4, m_g, m_{\tilde{t}_1}, m_{\tilde{t}_1}, m_{\tilde{t}_1}] - \\
&\quad (2(D_{311} - D_{312} + D_{313}) + m_g^2(D_{26} - D_{25}) + 2m_{\tilde{t}_1}^2(D_{310} - D_{35}) + \\
&\quad \quad 2(p_1 \cdot p_2)(2D_{25} - 2D_{26} - D_{310} + D_{35}) + \\
&\quad \quad 2(p_1 - p_2) \cdot p_4(D_{310} - D_{37} - D_{38} + D_{39})) \\
&\quad \left. [p_1, -p_4, -p_3, m_g, m_{\tilde{t}_1}, m_{\tilde{t}_1}, m_{\tilde{t}_1}] \right\}
\end{aligned} \tag{A3}$$

$$f_{vir,4}^{(g)} = f_3^{(g)}(\hat{t} \rightarrow \hat{u}, p_3 \leftrightarrow p_4) \tag{A4}$$

$$\begin{aligned}
f_{vir,5}^{(g)} &= -\frac{g_s^2 C_F}{4\pi^2} \left\{ (2C_0 + 3C_{11} - C_{12} + C_{21} - C_{23})[p_1, -p_3, m_g, m_{\tilde{t}_1}, m_{\tilde{t}_1}] \right. \\
&\quad - (C_{12} - C_{23})[-p_3, -p_4, m_{\tilde{t}_1}, m_{\tilde{t}_1}, m_{\tilde{t}_1}] \\
&\quad + (m_g^2(D_{13} + D_{26}) + 2m_{\tilde{t}_1}^2(D_{25} + D_{310}) - 2(D_{27} + D_{312} + D_{313}) + \\
&\quad \quad 2(p_1 - p_2) \cdot p_3(D_{23} - D_{26} - D_{38} + D_{39}) - \\
&\quad \quad 2(p_1 \cdot p_2)(2D_{13} + D_{25} + 2D_{26} + D_{310})) \\
&\quad \left. [p_1, -p_3, -p_4, m_g, m_{\tilde{t}_1}, m_{\tilde{t}_1}, m_{\tilde{t}_1}] \right\} \\
&+ (p_3 \leftrightarrow p_4)
\end{aligned} \tag{A5}$$

The form factors $f_i^{(\tilde{g})}$ due to the gluino exchange can be expressed as

$$\begin{aligned}
f_1^{(\tilde{g})} = & \frac{g_s^2 C_F}{16\pi^2} \{d \cdot B_0[-p_4, m_t, m_t] \\
& - 2(d \cdot C_{24} + 2m_{\tilde{g}}^2 C_0 + 2m_{\tilde{t}_1}^2 C_{12} + 2(p_1 \cdot p_2)(C_0 + C_{12}) + \\
& \quad 2(p_2 \cdot p_3)(C_0 + C_{11}) + 2(p_1 \cdot p_3)C_{12} + m_t m_{\tilde{g}} \sin 2\theta_{\tilde{t}} C_0) \\
& \quad [-p_3, -p_4, m_t, m_t, m_t] \\
& - 4(m_{\tilde{g}}^2(m_t^2 - m_{\tilde{g}}^2)D_0 - 2(m_t^2 + m_{\tilde{g}}^2)D_{27} + \\
& \quad m_{\tilde{t}_1}^2(m_t^2 D_{13} + m_{\tilde{g}}^2(D_{13} - D_0 - 2D_{11}) + m_{\tilde{t}_1}^2(2D_{23} - D_{13} - 2D_{25})) + \\
& \quad (p_1 \cdot p_2)(m_t^2(D_{13} - D_{11}) - 4D_{27} + m_{\tilde{g}}^2(D_{11} + D_{13}) + \\
& \quad \quad m_{\tilde{t}_1}^2(D_{11} - D_{13} + 2D_{21} + 4D_{23} - 4D_{25})) + \\
& \quad (p_1 \cdot p_3)(m_t^2(D_{11} - D_{13}) + m_{\tilde{g}}^2(D_0 + D_{11} + 2D_{12} - 3D_{13}) + \\
& \quad \quad m_{\tilde{t}_1}^2(D_{13} - 2D_{23} + 2D_{26})) + \\
& \quad (p_2 \cdot p_3)(m_t^2(D_{12} - 2D_{13}) - m_{\tilde{g}}^2(D_0 + D_{12}) + \\
& \quad \quad m_{\tilde{t}_1}^2(2D_{13} - D_{11} - D_{12} - 2D_{23} - 2D_{24} + 2D_{25} + 2D_{26})) + \\
& \quad 2(p_1 \cdot p_2)^2(D_{23} - D_{25}) + 2(p_1 \cdot p_2)(p_2 \cdot p_3)(D_{26} - D_{23}) + \\
& \quad 2(p_1 \cdot p_2)(p_1 \cdot p_3)(D_{25} + D_{26} - D_{23} - D_{24}) + \\
& \quad 2(p_1 \cdot p_3)(p_2 \cdot p_3)(D_{12} - D_{13} + D_{22} + D_{23} - 2D_{26}) + \\
& \quad m_t m_{\tilde{g}} \sin 2\theta_{\tilde{t}} ((m_t^2 - m_{\tilde{g}}^2)D_0 - 4D_{27} + m_{\tilde{t}_1}^2(2D_{13} - D_0 - 2D_{11}) + \\
& \quad \quad 2(p_1 \cdot p_2)D_{13} - (p_2 \cdot p_3)(D_0 + 2D_{13}) + \\
& \quad \quad (p_1 \cdot p_3)(D_0 + 2D_{11} + 2D_{12} - 4D_{13}))) \\
& \quad [p_1, -p_3, -p_4, m_{\tilde{g}}, m_t, m_t, m_t]\} \\
& + (p_3 \leftrightarrow p_4) + 2 \delta Z^{(\tilde{g})}
\end{aligned} \tag{A6}$$

$$\begin{aligned}
f_2^{(\tilde{g})} = & \frac{g_s^2 C_F}{4\pi^2} \{(C_{12} + 2C_{23})[-p_3, -p_4, m_t, m_t, m_t] \\
& - (m_{\tilde{t}}^2(D_{11} - 2D_{12} + D_{13} + 2D_{21} - 2D_{24} - 2D_{25} + 2D_{26}) + \\
& \quad m_{\tilde{g}}^2(D_0 + 3D_{11} - 2D_{12} - D_{13} + 2D_{21} - 2D_{24} - 2D_{25} + 2D_{26}) + \\
& \quad m_{\tilde{t}_1}^2(D_{13} - 2D_{23} + 2D_{25}) + \\
& \quad 2((p_1 \cdot p_2) - (p_2 \cdot p_3))(D_{13} - D_{12} - D_{23} - D_{24} + D_{25} + D_{26}) + \\
& \quad m_t m_{\tilde{g}} \sin 2\theta_{\tilde{t}}(D_0 + 4(D_{11} - D_{12} + D_{21} - D_{24} - D_{25} + D_{26}))) \\
& \quad [p_1, -p_3, -p_4, m_{\tilde{g}}, m_t, m_t, m_t]\} \\
& + (p_3 \leftrightarrow p_4)
\end{aligned} \tag{A7}$$

$$\begin{aligned}
f_3^{(\tilde{g})} &= \frac{d \cdot g_s^2 C_F}{4\pi^2 (\hat{t} - m_{\tilde{t}_1}^2)^2} \left\{ ((m_{\tilde{g}}^2 + m_t m_{\tilde{g}} \sin 2\theta_{\tilde{t}}) B_0 + \hat{t} \cdot B_1) [p_1 - p_3, m_{\tilde{g}}, m_t] - A_0[m_t] \right\} \\
&+ \frac{g_s^2 C_F}{4\pi^2 (\hat{t} - m_{\tilde{t}_1}^2)^2} \left\{ d \cdot B_0[-p_3, m_t, m_t] + 4 \cdot (2(p_1, p_3) C_{12} - m_t^2 C_{11} - \right. \\
&\quad \left. m_{\tilde{g}}^2 \cdot (2C_0 + C_{11}) - m_{\tilde{t}_1}^2 C_{11} - \right. \\
&\quad \left. 2m_t m_{\tilde{g}} \sin 2\theta_{\tilde{t}} (C_0 + C_{11})) [p_1, -p_3, m_{\tilde{g}}, m_t, m_t] \right\} \\
&- \frac{4}{(\hat{t} - m_{\tilde{t}_1}^2)^2} (\hat{t} \cdot \delta Z^{(\tilde{g})} - \delta M^{2(\tilde{g})} - m_{\tilde{t}_1}^2 \cdot \delta Z^{(\tilde{g})}) + \frac{8}{\hat{t} - m_{\tilde{t}_1}^2} \delta Z^{(\tilde{g})} \\
&+ \frac{g_s^2 C_F}{4\pi^2} \left\{ (C_0 + C_{11} + 3C_{12} + 4C_{23}) [-p_3, -p_4, m_t, m_t, m_t] \right. \\
&\quad - (2m_{\tilde{t}}^2 (D_{13} - D_{11} - D_{12} - D_{24} + D_{26}) - m_{\tilde{t}_1}^2 D_{11} + \\
&\quad \left. m_{\tilde{g}}^2 (2(D_{13} - D_{11} - D_{12} - D_{24} + D_{26}) - 3D_0) + \right. \\
&\quad \left. 2(p_1 \cdot p_2)(D_{13} - D_{12} - D_{24} + D_{26}) + 2(p_1 \cdot p_3)(D_{12} - D_{13}) + \right. \\
&\quad \left. m_t m_{\tilde{g}} \sin 2\theta_{\tilde{t}} (4(D_{13} - D_{11} - D_{12} - D_{24} + D_{26}) - 3D_0)) \right. \\
&\quad \left. [p_1, -p_3, -p_4, m_{\tilde{g}}, m_t, m_t, m_t] \right. \\
&\quad - (m_{\tilde{g}}^2 (D_0 - D_{11} + D_{12} - D_{13} - 2D_{25} + 2D_{26}) + 4D_{27} + \\
&\quad \left. m_t^2 (D_{11} - D_{12} + D_{13} - 2D_{25} + 2D_{26}) + \right. \\
&\quad \left. m_{\tilde{t}_1}^2 (D_{12} - D_{13} - 2D_{21} - 2D_{23} + 2D_{24} + 2D_{25} - 2D_{26}) + \right. \\
&\quad \left. 2(p_1 \cdot p_2)(D_{25} - D_{23}) + 2(p_2 \cdot p_4)(D_{23} - D_{26}) + \right. \\
&\quad \left. 2(p_1 \cdot p_4)(D_{13} - D_{12} - D_{22} + D_{24} - D_{25} + D_{26}) + \right. \\
&\quad \left. m_t m_{\tilde{g}} \sin 2\theta_{\tilde{t}} (D_0 - 4D_{25} + 4D_{26})) \right. \\
&\quad \left. [p_1, -p_4, -p_3, m_{\tilde{g}}, m_t, m_t, m_t] \right\}
\end{aligned} \tag{A8}$$

$$f_4^{(\tilde{g})} = f_3^{(\tilde{g})}(\hat{t} \rightarrow \hat{u}, p_3 \leftrightarrow p_4) \tag{A9}$$

$$\begin{aligned}
f_5^{(\tilde{g})} &= \frac{g_s^2 C_F}{4\pi^2} \left\{ (C_0 + C_{11} + 2C_{12} + 2C_{23}) [-p_3, -p_4, m_t, m_t, m_t] \right. \\
&\quad - (m_{\tilde{t}_1}^2 (D_{11} + D_{12} - 2D_{13} + 2D_{24} - 2D_{26}) + \\
&\quad \left. m_{\tilde{g}}^2 (D_0 + D_{12} + 2D_{13} + 2D_{26}) + \right. \\
&\quad \left. m_t^2 (2D_{13} - D_{12} + 2D_{26}) + \right. \\
&\quad \left. 2(p_1 \cdot p_3)(D_{13} - D_{12} - D_{22} + D_{26}) + \right. \\
&\quad \left. m_t m_{\tilde{g}} \sin 2\theta_{\tilde{t}} (D_0 + 4D_{13} + 4D_{26})) \right. \\
&\quad \left. [p_1, -p_3, -p_4, m_{\tilde{g}}, m_t, m_t, m_t] \right\} \\
&+ (p_3 \leftrightarrow p_4)
\end{aligned} \tag{A10}$$

The factors arising from the contribution of squark quartic interactions, are given as

follow

$$f_1^{(\hat{t})} = \frac{g_s^2}{6\pi^2} \cos^2 2\theta_{\hat{t}} \left\{ 4 \cdot C_{24}[-p_3, p_3 + p_4, m_{\hat{t}_1}, m_{\hat{t}_1}, m_{\hat{t}_1}] - B_0[p_1 + p_2, m_{\hat{t}_1}, m_{\hat{t}_1}] \right\} + (\cos \rightarrow \sin, m_{\hat{t}_1} \rightarrow m_{\hat{t}_2}) \quad (A11)$$

$$f_2^{(\hat{t})} = \frac{2g_s^2}{3\pi^2} \cos^2 2\theta_{\hat{t}} (C_{23} - C_{22})[-p_3, p_3 + p_4, m_{\hat{t}_1}, m_{\hat{t}_1}, m_{\hat{t}_1}] + (\cos \rightarrow \sin, m_{\hat{t}_1} \rightarrow m_{\hat{t}_2}) \quad (A12)$$

$$f_3^{(\hat{t})} = \frac{2g_s^2}{3\pi^2} \cos^2 2\theta_{\hat{t}} (C_{23} - C_{22})[-p_3, p_3 + p_4, m_{\hat{t}_1}, m_{\hat{t}_1}, m_{\hat{t}_1}] + (\cos \rightarrow \sin, m_{\hat{t}_1} \rightarrow m_{\hat{t}_2}) \quad (A13)$$

$$f_4^{(\hat{t})} = f_3^{(\hat{t})}(\hat{t} \rightarrow \hat{u}) \quad (A14)$$

$$f_5^{(\hat{t})} = f_2^{(\hat{t})} \quad (A15)$$

The factors shown in Eq.(3.11b) have the expressions as

$$\begin{aligned} f_{real}^{\hat{t}\hat{t}} &= 2 \cdot I_2 - m_{\hat{t}_1}^2 \cdot (I_{11} + I_{22}) + 2(p_1 \cdot p_2) \cdot I_{12} \\ &- \frac{2m_{\hat{t}_1}^2}{(p_1 \cdot p_2)}(I_1 + I_2) + \frac{2m_{\hat{t}_1}^2}{(p_1 \cdot p_3)}I_1 + \frac{2(p_3 - p_1) \cdot p_2}{(p_1 \cdot p_3)}I_2 \\ &- \frac{2m_{\hat{t}_1}^2}{(p_1 \cdot p_2)^2} - \frac{m_{\hat{t}_1}^2}{(p_1 \cdot p_3)^2} + \frac{2m_{\hat{t}_1}^2}{(p_1 \cdot p_2)(p_1 \cdot p_3)} + \frac{2(p_2 \cdot p_3)}{(p_1 \cdot p_2)(p_1 \cdot p_3)} \end{aligned} \quad (A16)$$

$$f_{real}^{\hat{u}\hat{u}} = f_{real}^{\hat{t}\hat{t}}(p_3 \rightarrow p_4) \quad (A17)$$

$$f_{real}^{\hat{q}\hat{q}} = 2(p_1 \cdot p_2)I_{12} - m_{\hat{t}_1}^2 (I_{11} + I_{22}) \quad (A18)$$

$$\begin{aligned} f_{real}^{\hat{t}\hat{u}} &= 2 \cdot I_2 - m_{\hat{t}_1}^2 \cdot (I_{11} + I_{22}) + 2(p_1 \cdot p_2) \cdot I_{12} \\ &- \frac{2m_{\hat{t}_1}^2}{(p_1 \cdot p_2)}(I_1 + I_2) + \frac{m_{\hat{t}_1}^2}{(p_1 \cdot p_3)}I_1 + \frac{m_{\hat{t}_1}^2}{(p_1 \cdot p_4)}I_1 + \frac{(p_3 - p_1) \cdot p_2}{(p_1 \cdot p_3)}I_2 + \frac{(p_4 - p_1) \cdot p_2}{(p_1 \cdot p_4)}I_2 \\ &- \frac{2m_{\hat{t}_1}^2}{(p_1 \cdot p_2)^2} + \frac{m_{\hat{t}_1}^2}{(p_1 \cdot p_2)(p_1 \cdot p_3)} + \frac{m_{\hat{t}_1}^2}{(p_1 \cdot p_2)(p_1 \cdot p_4)} \\ &- \frac{m_{\hat{t}_1}^2}{(p_1 \cdot p_3)(p_1 \cdot p_4)} + \frac{(p_2 \cdot p_3)}{(p_1 \cdot p_2)(p_1 \cdot p_3)} + \frac{(p_2 \cdot p_4)}{(p_1 \cdot p_2)(p_1 \cdot p_4)} - \frac{(p_3 \cdot p_4)}{(p_1 \cdot p_3)(p_1 \cdot p_4)} \end{aligned} \quad (A19)$$

$$\begin{aligned} f_{real}^{\hat{q}\hat{t}} &= I_2 - m_{\hat{t}_1}^2 \cdot (I_{11} + I_{22}) + 2(p_1 \cdot p_2) \cdot I_{12} \\ &+ \frac{m_{\hat{t}_1}^2}{(p_1 \cdot p_3)}I_1 - \frac{m_{\hat{t}_1}^2}{(p_1 \cdot p_2)}I_1 - \frac{m_{\hat{t}_1}^2}{(p_1 \cdot p_2)}I_2 + \frac{(p_3 - p_1) \cdot p_2}{(p_1 \cdot p_3)}I_2 \end{aligned} \quad (A20)$$

$$f_{real}^{\hat{q}\hat{u}} = f_{real}^{\hat{q}\hat{t}}(p_3 \rightarrow p_4) \quad (A21)$$

with

$$I_{ab\dots} = \frac{1}{(p_a \cdot k)(p_b \cdot k)\dots} \quad (a, b = 1, 2) \quad (A22)$$

References

- [1] S.L. Glashow, Nucl. Phys. 22(1961)579; S. Weinberg, Phys. Rev. Lett. 1(1967)1264; A. Salam, Proc. 8th Nobel Symposium Stockholm 1968, ed. N. Svartholm(Almquist and Wiksells, Stockholm 1968) p.367; H.D. Politzer, Phys. Rep. 14(1974)129.
- [2] P.W. Higgs, Phys. Lett 12(1964)132, Phys. Rev. Lett. 13 (1964)508; Phys.Rev. 145(1966)1156; F.Englert and R.Brout, Phys. Rev. Lett. 13(1964)321; G.S. Guralnik, C.R.Hagen and T.W.B. Kibble, Phys. Rev. Lett. 13(1964)585; T.W.B. Kibble, Phys. Rev. 155(1967)1554.
- [3] H.E. Haber and G.L. Kane, Phys. Rep. 117(1985)75.
- [4] J.Ellis and S.Rudaz, Phys. Lett. B128(1983)248; J.F.Gunion and H.E.Haber, Nucl. Phys. B272(1986)1.
- [5] K.Hikasa and M.Kobayashi, Phys. Rev. D36(1987)724.
- [6] W.Beenakker, R.Hopker and P.M.Zerwas, Phys. Lett. B349(1995)463; A.Arhib, M.Capdequi-Peyranere and A.Djouadi, Phys. Rev D52(1995)1404; H.Eberl, A.Bartl and W.Majeroto, hep-ph/9603206.
- [7] I.F. Ginzburg, G.L. Kotkin, V.G. Serbo and V.I. Telnov, Pis'ma ZHETF 34(1981)514; Nucl. Instr. Methods 205(1983)47. Han Liang, Chong-Sheng Li and Ma Wen-Gan, Phys. Rev. D54(1996)2363.
- [8] A.Denner, Fortsch. Phys. Vol.41, No.4 (1993)

- [9] Bernd A.Kniehl, Phys. Rep. 240(1994)211.
- [10] L3 Collaboration, CERN-PPE/96-29(Submitted to Phys. Lett.B)
- [11] R.Blankenbecler and S.D.Drell, Phys. Rev. Lett. 61(2324)1988; F.Halzen, C.S.Kim and M.L.Stong, Phys. Lett. B274(489)1992; M.Drees and R.M.Godbole, Phys. Lett. 67(1189)1991.
- [12] V.Telnov, Nucl. Instr. Methods A294(72)1990.

Figure Captions

Fig.1 Feynman diagrams including the contributions from the tree-level and next-to-leading order in Supersymmetric QCD for $\gamma\gamma \rightarrow \tilde{t}_1\bar{\tilde{t}}_1$ process: (1-a) tree level diagrams; (1-b) corrections due to gluon contribution; (1-c) soft gluon emission; (1-d) corrections due to the pure supersymmetric particle \tilde{g} and \tilde{t}_i . The diagrams by exchanging initial photons are not shown here.

Fig.2 When $m_{\tilde{g}} = 250 \text{ GeV}$, $m_{\tilde{t}_1} = 200 \text{ GeV}$, $m_{\tilde{t}_2} = 550 \text{ GeV}$ and $\cos\theta_{\tilde{t}} = 0.7$: (a) the cross section $\hat{\sigma}(\gamma\gamma \rightarrow \tilde{t}_1\bar{\tilde{t}}_1)$ as a function of $\sqrt{\hat{s}}$, solid-line for tree-level contribution $\hat{\sigma}_B$, dotted-line for the conventional QCD correction $\hat{\sigma}^{(g)}$, dashed-line for the pure supersymmetric particle QCD contribution $\hat{\sigma}^{(\tilde{g}+\tilde{t})}$; (b) the cross section $\sigma(e^+e^- \rightarrow \gamma\gamma \rightarrow \tilde{t}_1\bar{\tilde{t}}_1)$ as a function of \sqrt{s} , solid-line for tree level contribution σ_B , dash-dotted-line for the overall QCD correction $\sigma^{(g+\tilde{g}+\tilde{t})}$.

Fig.3 The cross section $\hat{\sigma}$ as a function of $m_{\tilde{t}_1}$, when $\sqrt{\hat{s}} = 1000 \text{ GeV}$, $m_{\tilde{t}_2} = 550 \text{ GeV}$, $m_{\tilde{g}} = 250 \text{ GeV}$ and $\cos\theta_{\tilde{t}} = 0.7$: solid-line for tree-level contribution $\hat{\sigma}_B$, dotted-line for the conventional QCD correction $\hat{\sigma}^{(g)}$, dashed-line for the pure supersymmetric particle QCD contribution $\hat{\sigma}^{(\tilde{g}+\tilde{t})}$.

Fig.4 The relative correction $\delta\hat{\sigma}/\hat{\sigma}_B$ as a function of $m_{\tilde{t}_2}$, when $\sqrt{\hat{s}} = 500 \text{ GeV}$, $m_{\tilde{t}_1} = 200 \text{ GeV}$, $m_{\tilde{g}} = 250 \text{ GeV}$ and $\cos\theta_{\tilde{t}} = 0.7$: dotted-line for the contribution $\delta\hat{\sigma}^{(g+\tilde{g})}/\hat{\sigma}_B$, dashed-line for the QCD correction due to squark quartic interactions $\delta\hat{\sigma}^{(\tilde{t})}/\hat{\sigma}_B$.

Fig.5 The relative correction $\delta\hat{\sigma}/\hat{\sigma}_B$ as a function of $m_{\tilde{g}}$, when $\sqrt{\hat{s}} = 500 \text{ GeV}$, $m_{\tilde{t}_1} = 200 \text{ GeV}$, $m_{\tilde{t}_2} = 550 \text{ GeV}$ and $\cos\theta_{\tilde{t}} = 0.7$: dotted-line for the contribution $\delta\hat{\sigma}^{(g+\tilde{t})}/\hat{\sigma}_B$, dashed-line for the QCD correction due to the gluino exchange $\delta\hat{\sigma}^{(\tilde{g})}/\hat{\sigma}_B$.

Fig.6 The relative correction $\delta\hat{\sigma}/\hat{\sigma}_B$ as a function of $\cos\theta_{\tilde{t}}$, when $\sqrt{\hat{s}} = 500 \text{ GeV}$, $m_{\tilde{t}_1} = 200 \text{ GeV}$, $m_{\tilde{t}_2} = 550 \text{ GeV}$ and $m_{\tilde{g}} = 250 \text{ GeV}$: dotted-line for the gluon contribution $\delta\hat{\sigma}^{(g)}/\hat{\sigma}_B$, dash-line for the pure supersymmetric particle contribution $\delta\hat{\sigma}^{(\tilde{g}+\tilde{t})}/\hat{\sigma}_B$.

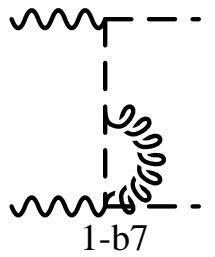
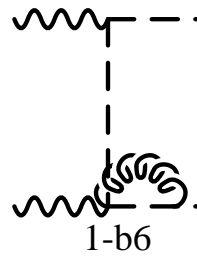
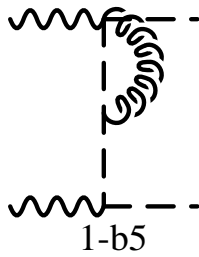
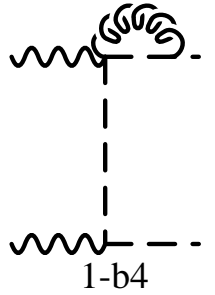
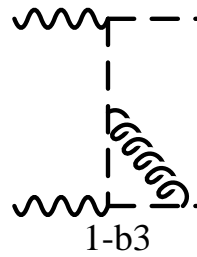
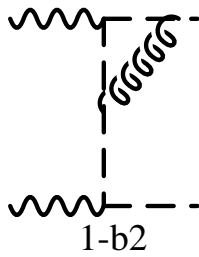
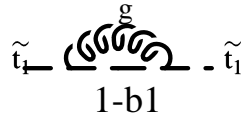
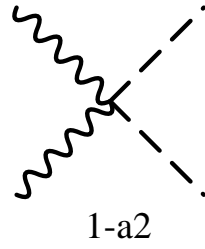
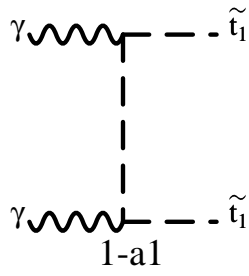


Fig.1 (continued)

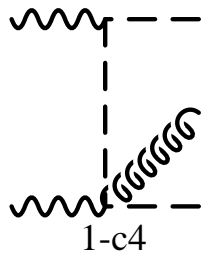
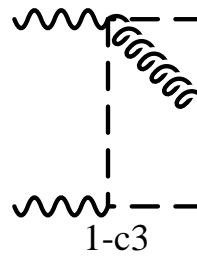
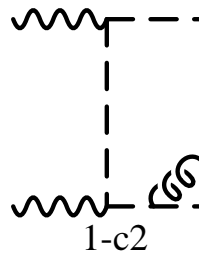
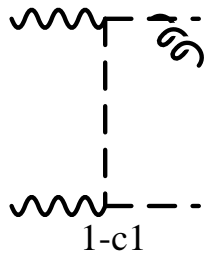
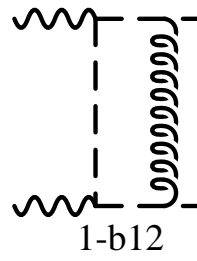
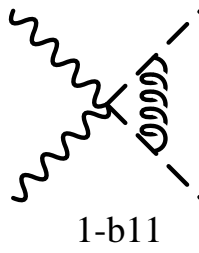
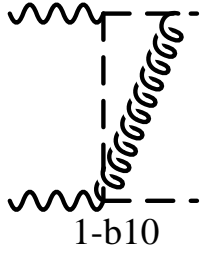
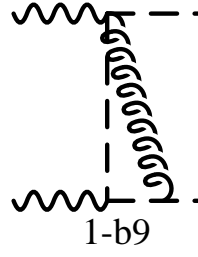
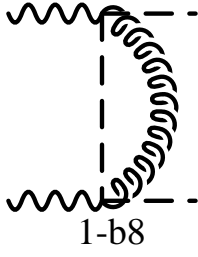


Fig.1 (continued)

Fig.2(a)

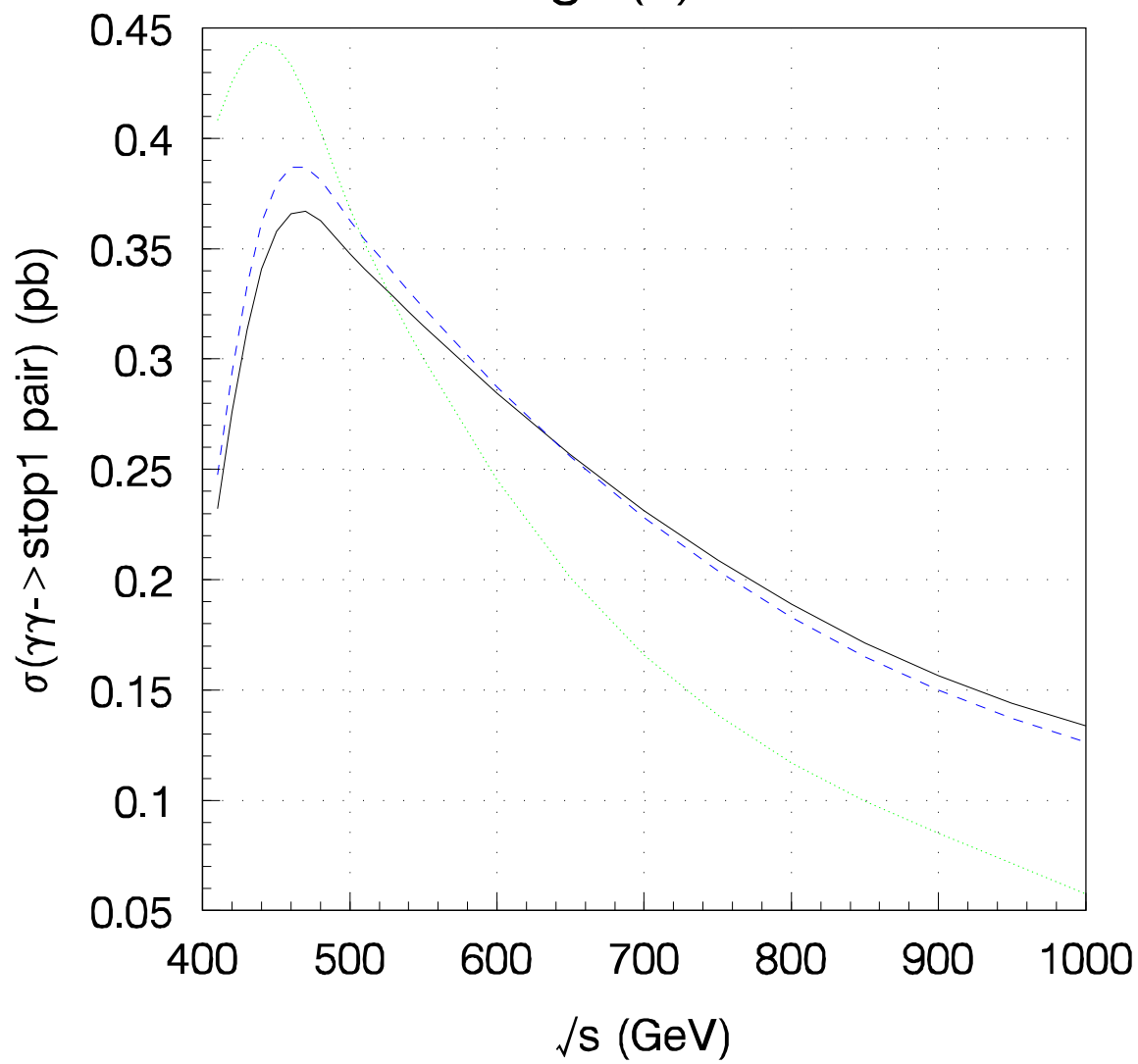
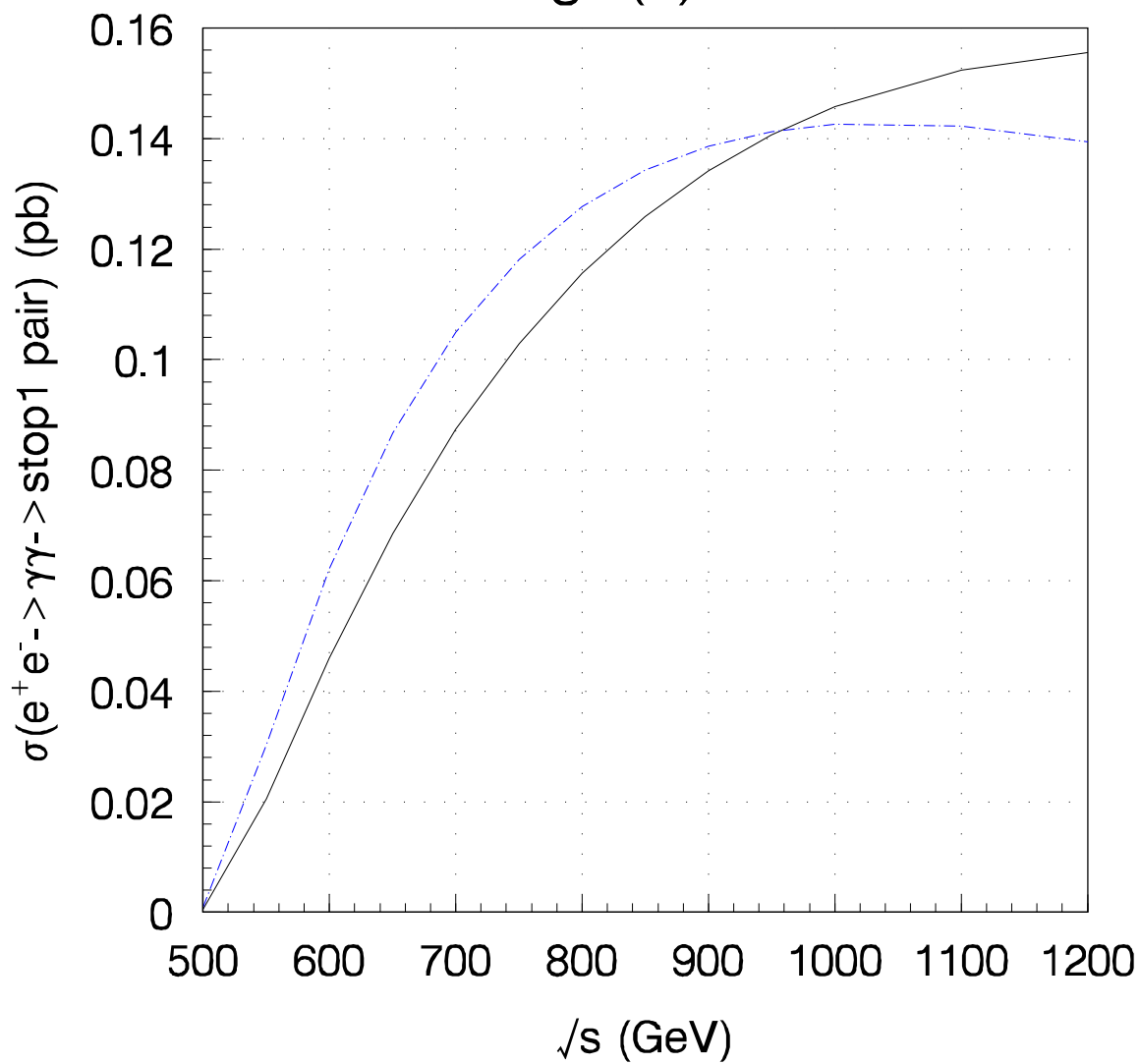


Fig.2(b)



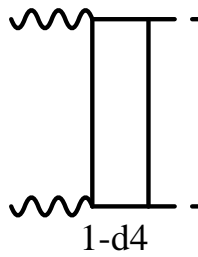
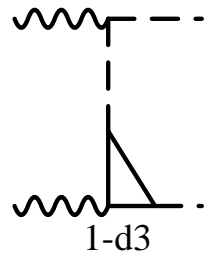
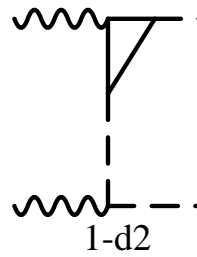
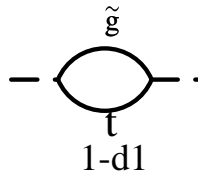
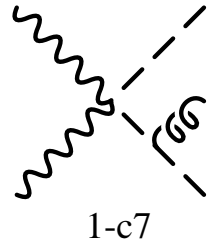
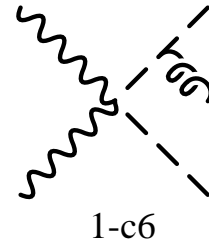
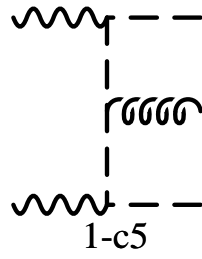
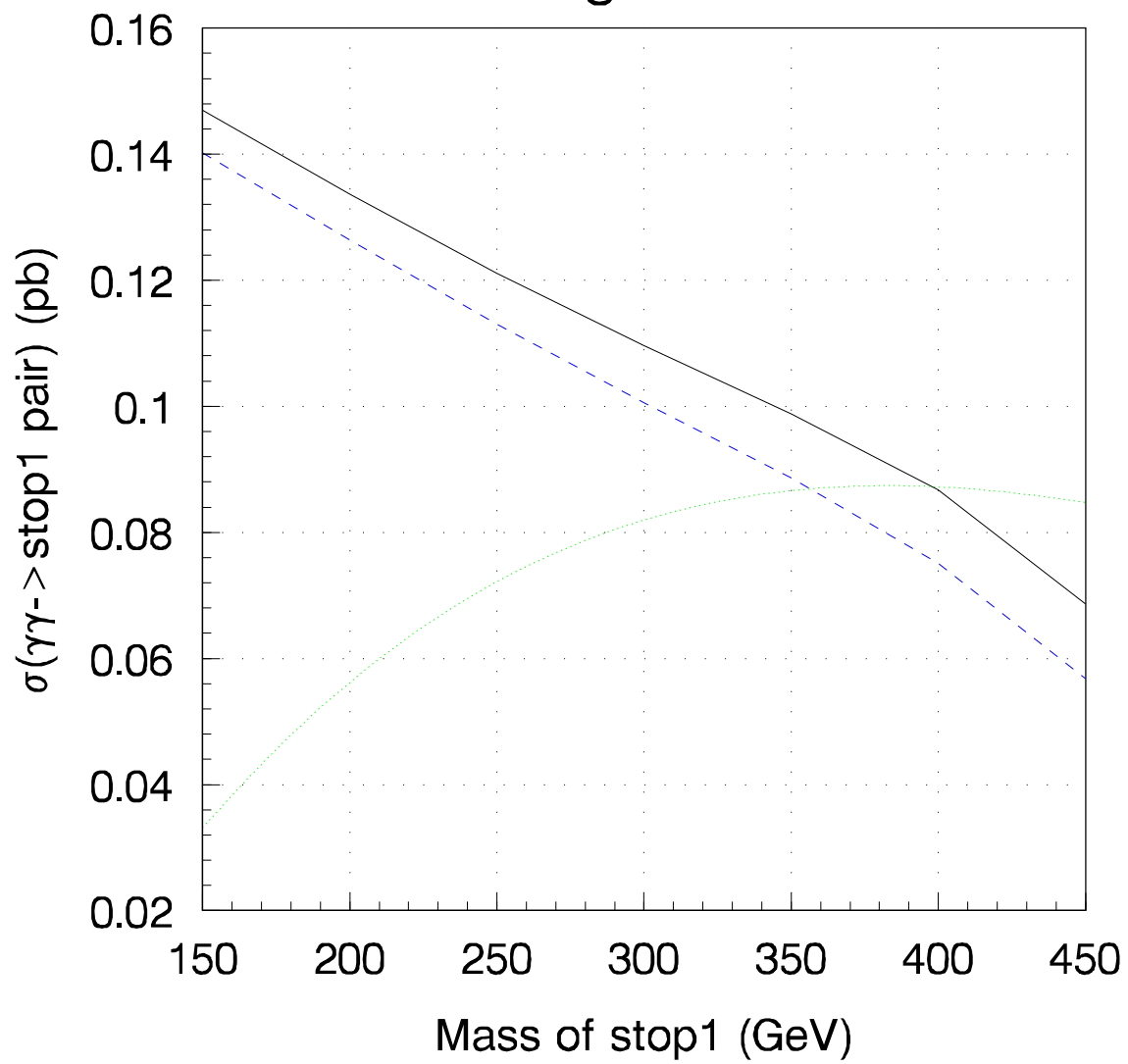


Fig.1 (continued)

Fig.3



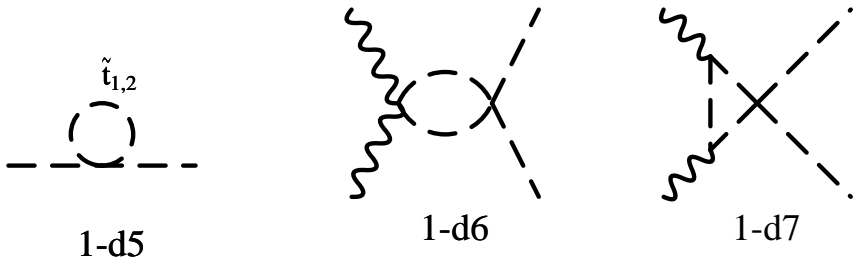


Fig.1 (finished)

Fig.4

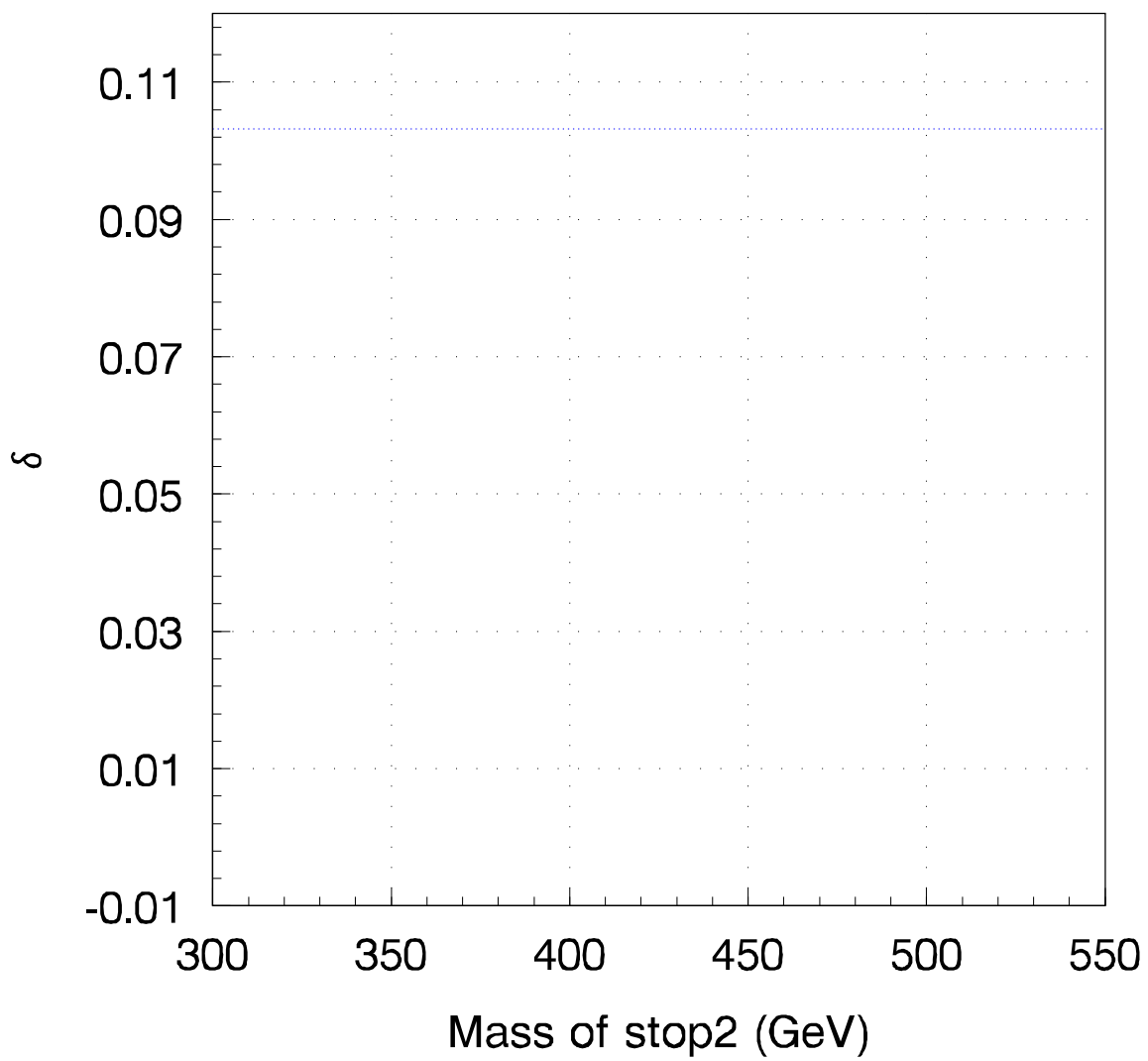


Fig.5

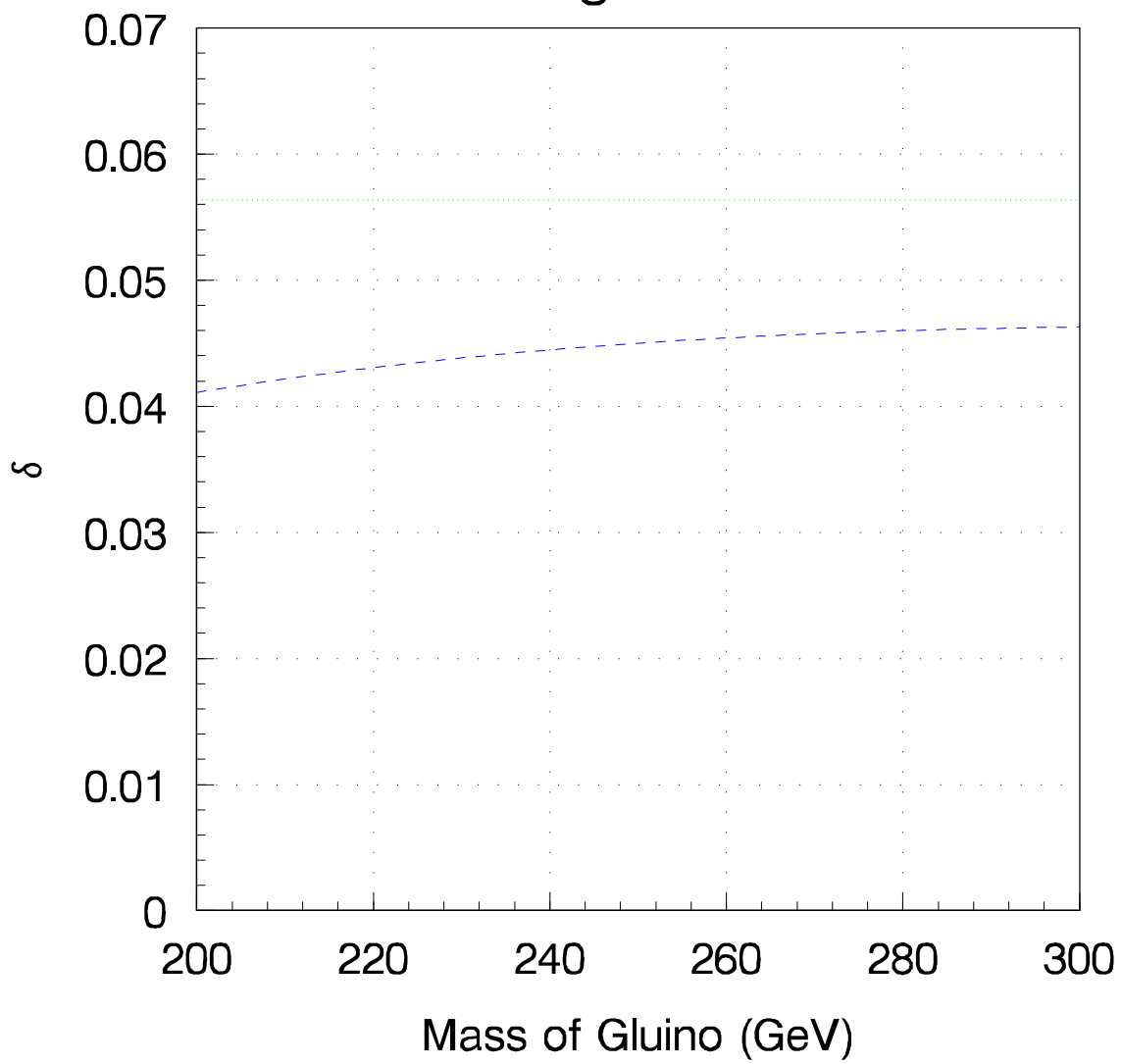


Fig.6

